







ARTICLE



Sulfate differentially stimulates but is not respired by diverse anaerobic methanotrophic archaea

Hang Yu ¹, Connor T. Skennerton ¹, Grayson L. Chadwick¹, Andy O. Leu², Masataka Aoki ^{3,4}, Gene W. Tyson ² and Victoria J. Orphan ¹ 

© The Author(s), under exclusive licence to International Society for Microbial Ecology 2021, corrected publication 2021

Sulfate-coupled anaerobic oxidation of methane (AOM) is a major methane sink in marine sediments. Multiple lineages of anaerobic methanotrophic archaea (ANME) often coexist in sediments and catalyze this process syntrophically with sulfate-reducing bacteria (SRB), but the potential differences in ANME ecophysiology and mechanisms of syntrophy remain unresolved. A humic acid analog, anthraquinone 2,6-disulfonate (AQDS), could decouple archaeal methanotrophy from bacterial sulfate reduction and serve as the terminal electron acceptor for AOM (AQDS-coupled AOM). Here in sediment microcosm experiments, we examined variations in physiological response between two co-occurring ANME-2 families (ANME-2a and ANME-2c) and tested the hypothesis of sulfate respiration by ANME-2. Sulfate concentrations as low as 100 μM increased AQDS-coupled AOM nearly 2-fold matching the rates of sulfate-coupled AOM. However, the SRB partners remained inactive in microcosms with sulfate and AQDS and neither ANME-2 families respired sulfate, as shown by their cellular sulfur contents and anabolic activities measured using nanoscale secondary ion mass spectrometry. ANME-2a anabolic activity was significantly higher than ANME-2c, suggesting that ANME-2a was primarily responsible for the observed sulfate stimulation of AQDS-coupled AOM. Comparative transcriptomics showed significant upregulation of ANME-2a transcripts linked to multiple ABC transporters and downregulation of central carbon metabolism during AQDS-coupled AOM compared to sulfate-coupled AOM. Surprisingly, genes involved in sulfur anabolism were not differentially expressed during AQDS-coupled AOM with and without sulfate amendment. Collectively, this data indicates that ANME-2 archaea are incapable of respiring sulfate, but sulfate availability differentially stimulates the growth and AOM activity of different ANME lineages.

The ISME Journal (2022) 16:168–177; <https://doi.org/10.1038/s41396-021-01047-0>


INTRODUCTION

Sulfate-coupled anaerobic oxidation of methane (AOM) is a microbial process that consumes >90% of the annual methane flux from marine sediments [1, 2]. A symbiosis between anaerobic methanotrophic archaea (ANME) and sulfate-reducing bacteria (SRB) catalyze sulfate-coupled AOM. Since the discovery of these consortia two decades ago, diverse ANME lineages (e.g. ANME-1a/1b/2a/2b/2c/3) have been recognized to form partnership with different SRB lineages (e.g. HotSeep-1, SEEP-SRB1a/1g) [1, 3–7]. These lineages represent different species, genera, families and even orders, and encode an extensive pangenome [4, 8]. This phylogenetic and genomic diversity likely promotes differences in the metabolic properties, symbiotic interactions, and ecological adaptation among AOM consortia in methane seep ecosystems.

Sulfur is integral to AOM consortia for multiple reasons. As the predominant terminal electron acceptor for AOM in marine environments, sulfate is generally thought to be reduced by the SRB partners [1]. It has also been proposed that sulfate is respired by ANME [9] in ANME-2a/2c and SEEP-SRB1a symbiosis [10]. In this hypothesized syntrophic mechanism, sulfate reduction by ANME-2

generates zero-valent sulfur as a diffusible intermediate that is subsequently disproportionated by their SEEP-SRB1a partner. While subsequent genomic, modeling and cultivation studies do not support transfer of zero-valent sulfur between ANME and SRB [6, 8, 11–14], direct cellular sulfur content measurements to track accumulation of zero-valent sulfur during AOM as performed in the original study [9] have not been verified and experiments focused on ANME physiology independent of the activity of the bacterial partner have not been reported. Beyond microbial respiration, sulfur is an essential element in all organisms, comprising ~1% of a cell's biomass and plays a key role in many anabolic processes as a component of amino acids and coenzymes with sulfur oxidation states varying from +4 to –2 [15, 16]. Furthermore, organosulfur compounds are also produced as secondary metabolites and have been reported from ANME-1a consortia [17].

Previous work demonstrated that a humic acid analog, anthraquinone-2,6-disulfonate (AQDS), could serve as an alternative soluble electron acceptor for methane-derived electrons in lieu of syntrophic SRB partners [12]. In these experiments, ANME

¹Division of Geological and Planetary Sciences, California Institute of Technology, Pasadena, CA, USA. ²Centre for Microbiome Research, School of Biomedical Sciences, Queensland University of Technology, Translational Research Institute, Woolloongabba, Australia. ³Department of Civil Engineering, National Institute of Technology, Wakayama College, Gobo, Wakayama, Japan. ⁴Present address: Regional Environment Conservation Division, National Institute for Environmental Studies, Tsukuba, Ibaraki, Japan. email: vorphan@gps.caltech.edu

Received: 27 January 2021 Revised: 21 June 2021 Accepted: 22 June 2021

Published online: 20 July 2021

transferred methane-derived electrons via extracellular electron transfer (EET) to AQDS instead of their SRB partner, and remained anabolically active, with AOM activities ~80% of that with sulfate [12]. Also noted in the previous work, AQDS-coupled AOM was only possible in a sulfur-free medium [12]. The observed inhibitory effect of sulfur on AOM consortia was subsequently attributed to inhibitory concentrations of zero-valent sulfur generated when reduced sulfur species such as sulfide reacted with AQDS [11]. While these experiments demonstrated the ability of ANME-2 to oxidize methane coupled to AQDS reduction (AQDS-coupled AOM), it remains possible that ANME may also be capable of directly oxidizing methane with sulfate.

In order to disentangle the role of sulfate in ANME physiology and understand the potential metabolic differences among ANME-2 lineages, we conducted a series of replicated AOM sediment microcosm experiments amended with AQDS, sulfate, AQDS and sulfate, or no electron acceptor in tandem with stable isotope probing using lineage-specific fluorescence in situ hybridization and nanoscale secondary ion mass spectrometry (FISH-nanoSIMS) and comparative metatranscriptomics to resolve activity and expression differences among the dominant ANME-2 families. As sulfate does not react with AQDS to produce zero-valent sulfur, we were able to test the potential use of sulfate as an electron acceptor and anabolic sulfur source for the ANME-2 families during AQDS-coupled AOM. We evaluated the resulting metabolic, anabolic and transcriptional responses of two co-occurring ANME-2 lineages and their SRB partners in light of the two prevailing hypotheses for the AOM syntrophic mechanism: sulfate respiration by ANME-2 coupled to zero-valent sulfur transfer to a sulfur disproportionating SRB partner [9] and direct interspecies electron transfer [13, 14].

MATERIALS AND METHODS

Sample collection and microcosm setup

The methane seep sediment sample (sediment #7142 or PC61) was collected from the Santa Monica basin (lat. 33.78905, long. -118.66833, 860 m water depth) below a white microbial mat during a research cruise organized by the Monterey Bay Aquarium Research Institute on board the R/V Western Flyer using ROV Doc Ricketts on dive DR463 in May, 2013. The intact sediment core (~12 cm in length) was processed shipboard and stored at 4 °C in a heat-sealed mylar bag flushed with argon for ~5 min to remove headspace oxygen. In the shore-based laboratory, the sediment was transferred under a stream of N₂ into a 1 L Pyrex bottle, mixed with N₂ sparged 0.2 µm filter sterilized benthic seawater collected near the seep site (~1:2 ratio), and sealed with a butyl rubber stopper and secured with a screwcap. The bottle was supplied with a methane headspace (0.2 MPa) and incubated at 4 °C. This large incubation ran for ~30 months with periodic replacement of anoxic sterilized benthic seawater and 0.2 MPa methane headspace when sulfide levels became elevated above 20 mM. Prior to establishment of the smaller volume microcosm experiments, the sediment was washed three times with anoxic sterilized sulfate-free artificial seawater (ASW) [12] and incubated under 0.2 MPa methane headspace for 6 months to deplete potential electron acceptors in the sediment that could support AOM. Sample manipulations were done on ice in anaerobic chamber with N₂:H₂ (95:5) atmosphere. Further details on our initial sediment characterization, including microbial community composition, can be found in our previous publication [12].

Prior to setting up the microcosm experiments, the headspace was exchanged with N₂:CO₂ (80:20, 0.2 MPa) by flushing for 5 min and then incubated overnight at 4 °C to remove CH₄. Microcosms were setup in 30-mL sterile serum bottles (Wheaton, Millville, NJ, USA) capped with NaOH-washed black butyl rubber stoppers (Geo-Microbial Technologies, Inc., Ochelata, OK, USA) each containing 2 ml of wet sediment (wet sediment = sediment after settling for at least 48 h) and 8 ml of sulfate-free ASW. For incubations with methane, each serum bottle was sparged with N₂ for 5 min followed by flushing with unlabeled CH₄ for 2 min, prior to injecting 0.9 ml of ¹³CH₄ (99% ¹³C, Cambridge Isotope Laboratories). We previously determined this ¹³CH₄ stock contained 0.05 vol% ¹³CO₂ as an impurity [12], which contributed to an initial spike of ¹³C-DIC after ¹³CH₄ addition. For bottles with a N₂:CO₂ headspace instead of methane, N₂:CO₂ (80:20) gas

was used to sparge the bottles. Anoxic, 0.2 µm filter sterilized stocks of electron acceptors were then added to the bottles by injecting 2 ml of 2× concentrated sulfate-free ASW amended with 2 mM ¹⁵N-ammonium chloride (99% ¹⁵N, Cambridge Isotope Laboratories, Tewksbury, MA, USA) and unlabeled ammonium chloride (Sigma Chemicals, St. Louis, MO, USA) resulting in 40% final ¹⁵N label, 2 ml of 2.5 mM Na₂SO₄ (Macron Fine Chemicals, Allentown, PA, USA) in nanopure deionized water and/or 10 mM AQDS (anthraquinone-2,6-disulfonate, >98%, Sigma Chemicals). For bottles with no electron acceptor (methane only control), 2× sulfate-free ASW with ¹⁵N-ammonium were mixed with 2 ml of nanopure deionized water. Each experimental condition under methane was set up in replicates (Supplementary Table 1A). All bottles (total = 45) were incubated on ice for 1 h before 6 ml of well-mixed sediment slurry (containing 2 ml of wet sediment and 4 ml of sulfate-free ASW with unlabeled ammonium) was added to the each bottle using a N₂-flushed 10-ml syringe with 16-gauge needle and over pressured with CH₄ or N₂:CO₂ to 0.35 MPa.

Geochemistry

Geochemical measurements were performed on subsamples of the anoxic microcosms over a 9-day period. In all, 0.5 ml of supernatant was subsampled using a N₂-flushed 10-ml syringe with 23-gauge needle from each microcosm after 1.5 h (day 0), 24 h (day 1), 72 h (day 3), 144 h (day 6), and 216 h (day 9) after the initial setup (Supplementary Table 1A). Supernatants were filtered through a 0.22-µm syringe filter; 0.15 ml of the filtrate was immediately flash frozen in liquid N₂ for DIC measurement and stored at -20 °C. The remaining filtrate (ca. 0.3 ml) was injected into a 10-ml serum bottle (Wheaton) capped with blue butyl rubber stopper (Chemglass Life Sciences, Vineland, NJ, USA) that had been previously flushed with N₂ for 5 min. In an anaerobic chamber (N₂:H₂ = 95:5), the 10-ml serum bottles were opened and 50 µl of the filtrate was mixed with 450 µl of pH 2 anoxic seawater and measured spectrophotometrically by quantifying absorption at 428 nm compared to AQDS standards of known concentration reduced with dithionite. In all, 100 µl of the filtrate was preserved in 400 µl of 0.5 M zinc acetate solution and sulfide concentrations were later measured by quantifying the absorbance at 670 nm via the methylene blue 'Cline' method [18]. The remaining filtrate was flash frozen in liquid N₂ and stored in -20 °C. In total, 30 µl of this stock was used for sulfate quantification via ion chromatography (Dionex ICS-3000), using an AS-19 column and bicarbonate eluent.

To quantify the ¹³C-DIC production over time, the ¹³C isotope ratio of -20 °C stored DIC samples from all treatments and time points were measured using a GC-IR-MS GasBench II (Thermo Scientific, Waltham, MA, USA) as described in Scheller et al. [12]. We also determined ¹³C-methane from a subset of headspace samples after 9 days of incubation using ¹H-NMR spectroscopy (Varian Inova 600 MHz Spectrometer with inverse triple resonance probe) to aid in the quantification of the proportion of methane oxidized. Methane was dissolved in chloroform-d (99.8% D, Cambridge Isotope Laboratories) via a long 23-gauge needle and acquired at 600 MHz with a repetition time of 100 s. Atom percent ¹³C-methane was calculated using a line fit of the ¹²CH₄ and ¹³CH₄ with the software MestReNova v.14.1 (Mestrelab Research, Compostela, Spain).

iTag community analysis and metagenomic sequencing of bulk sediment

Illumina iTag 16S rRNA gene sequencing of the microbial assemblage in the starting incubation of #7142 was carried out using three -20 °C stored samples from the large sediment incubation collected during seawater replacement prior to establishment of the microcosm experiments (ca. 2 mL slurry). DNA was extracted using the DNeasy PowerSoil kit (Qiagen, Valencia, CA, USA) following the manufacturer's instructions, with the bead beating option using a FastPrep FP120 instrument (Thermo Electron Corporation, Milford, MA, USA) at a setting of 5.5 for 45 s instead of the 10 min vortex step in the manufacturer's protocol. PCR amplification, barcoding and sequencing of the 16S rRNA hypervariable region (V4-V5) was performed using PCR primers and amplification conditions as previously described [11]. Sequencing data was processed using QIIME v1.8.0 [19], clustered at 99% sequencing identity using UCLUST v7.0.1001 [20], and the taxonomic identity of the most abundant sequence in each cluster was assigned using a custom SILVA database modified from SILVA Ref NR 99 Database Release 115 [21, 22].

For metagenomic sequencing, DNA was extracted from -80 °C frozen sediment #7142 (ca. 2 mL slurry) using the FastDNA SPIN kit for soil (MPBio, Santa Ana, CA, USA) according to the manufacturer's protocol. DNA concentrations were quantified using the Quant-iT dsDNA HS assay kit

(Invitrogen) as per the manufacturer's instructions. The paired-end library was prepared from the extracted DNA using the Nextera XT DNA library preparation kit (Illumina, San Diego, CA, USA). The libraries were sequenced on a NextSeq500 (Illumina) platform at the University of Queensland, generating 2 × 150 bp paired-end reads with an average insert length of 300 bp. Sequence processing, assembly, and binning were performed as described previously for the ANME-2c genome S7142MS2 after trimming low-abundance reads [11]. Metagenome-assembled genomes (MAGs) were further refined based on GC content [23] and checked for quality using CheckM v1.0.6 [24]; however, with strain heterogeneity, multiple copies of a gene may be present in each genome bin likely originating from different strains of the same species. Metagenome contigs were annotated using Prodigal v2.6.2 [25], and MAGs were additionally annotated using the IMG [26] Microbial Genome Annotation and NCBI [27] Prokaryotic Genome Annotation Pipelines. Comparison of transporters were done using the Transporter Classification Database (<http://www.tcdb.org/>) [28]. To obtain the proportion of genome bins in the bulk metagenome, mapping was performed using BMap v37.93 (<https://sourceforge.net/projects/bbmap/>) with *minid* = 0.90 ambiguous = random settings. Additionally, contigs with partial genes of interest were extended individually by first mapping sequence reads with *bwa* v0.7.10 [29] and re-assembled using the Geneious software v9 (<https://www.geneious.com>).

FISH-nanoSIMS analysis

The supernatant from each microcosm incubation was first removed under anoxic conditions and saved for geochemical analysis (as described above). Samples for FISH-nanoSIMS analysis and for RNA sequencing (see RNA extraction and analysis) were then immediately prepared by injecting 8 ml of N₂-sparged Lifeguard Soil Preservation Solution (MoBio Laboratories, Carlsbad, CA, USA) into the serum bottle and thoroughly mixed on ice. In all, 1 ml of the Lifeguard-sediment mixture was subsampled and fixed in 1.33% paraformaldehyde at 4 °C for 2 h for FISH microscopy and nanoSIMS analysis. Microscopy samples were later washed twice with 1 × phosphate-buffered saline (PBS; 145 mM NaCl, 1.4 mM NaH₂PO₄, 8 mM Na₂HPO₄ at pH 7.4), resuspended in PBS:ethanol (1:1), and stored at −20 °C.

PFA-fixed AOM consortia were recovered and concentrated from the sediment matrix using Percoll density separation, followed by Technovit resin embedding and sectioning as described previously [14]. FISH hybridizations at 40% formamide concentration were carried out using microtome cut semi-thin sections (1 μm) following protocols in [14]. An oligonucleotide probe specific to ANME-2a was developed in this study (ANME-2a-828; 5'-GGTCGCACCGTCTGACACCT-3') guided by the SILVA Ref NR 99 Database Release 115 [21]. Empirical tests of the signal intensity and cross-reactivity of this new probe were carried out between 10 and 70% formamide. The tests determined that the optimal formamide concentration for the new ANME-2a probe was 60% for intact AOM aggregates but could be reduced to 40% for AOM consortia in thin sections. Oligonucleotide probes with fluorescent labels on both the 5' and 3' ends were used in FISH hybridizations: ANME-2a-828 dual labeled with Alexa488, ANME-2c-760 (5'-CGCCCCAGCTTCGTCC-3'; [30]) dual labeled with Cy3, and the DSS658 probe targeting bacteria affiliated with *Desulfosarcina-Desulfococcus* (5'-TCCACTTCCCTCTCCCAT-3'; [31]) dual labeled with Cy5 (Integrated DNA Technologies, USA). In all, 5 μg/ml of a DAPI-Citifluor mounting medium was added prior to epifluorescence microscopy on a BX51 epifluorescence microscope using a ×100 objective (Olympus, Center Valley, PA, USA). After FISH imaging, DAPI-Citifluor was washed off the thin sections using deionized water and prepared for nanoSIMS analysis.

NanoSIMS analysis targeted specific FISH identified consortia in thin sections on polylysine-coated glass using a CAMECA NanoSIMS 50 L housed in Caltech's microanalysis center. Samples were sputter-coated with gold to enhance conductivity prior to analysis and specific aggregates were identified by comparing with tiled mosaic images of the sections showing the spatial location of each consortium as described in McGlynn et al. [14]. Consortia were pre-sputtered with a focused primary Cs⁺ beam (100–1000 pA), followed by analysis using 2–4 pA for secondary ion image acquisition. Secondary ions ¹²C¹²C[−], ¹²C¹⁴N[−], ¹²C¹³N[−], and ³²S[−] were collected simultaneously for at least two image frames. Individual ion image frames were aligned using the ¹²C¹⁴N[−] ion, and corresponding FISH images were transformed to match that of the nanoSIMS ion images using Look@NanoSIMS v2015-09-06 [32]. Regions of interest (ROIs) corresponding to ANME or SRB cells were defined manually. The final ion counts per ROI was calculated by summing the ion counts over all image frames. Additional details on nanoSIMS sample preparation,

analysis, and data processing can be found in our previous publications [12, 14]. ¹⁵N atom percent values for each cell after ¹⁵N-ammonium assimilation was used as a proxy for anabolic activity and calculated from atom percent data using ions collected from the nanoSIMS as follows: $^{15}\text{N}^{12}\text{C}^{-} / (^{15}\text{N}^{12}\text{C}^{-} + ^{14}\text{N}^{12}\text{C}^{-}) \times 100$ [14].

RNA preservation, extraction, and analysis

After sampling 1 ml of the Lifeguard-sediment mixture for FISH-nanoSIMS (above), the rest of the mixture was kept at 4 °C overnight in the serum bottle to allow complete reaction of the LifeGuard solution with the sample. The mixtures were sampled from the bottles and pelleted the next day by centrifuging at 5250 × *g* for 20 min at 4 °C in 15-ml falcon tubes. The supernatant was discarded, and the remaining pellet was flash frozen in liquid N₂ and stored at −80 °C until RNA extraction.

RNA extraction and sequencing were performed on replicated microcosms after 3 and 9 days of incubation using commercial kits according to manufacturer's protocols. Sediment pellet preserved in LifeGuard solution were first thawed from −80 °C and RNA was extracted from microcosm samples (Supplementary Table 1B) using RNA PowerSoil Total RNA Isolation kit (MoBio Laboratories). Turbo DNA-free kit (Ambion, Austin, TX, USA) was used to remove genomic DNA and purified using RNeasy MinElute cleanup kit (Qiagen) and rRNA subtraction was performed using Ribo-Zero Magnetic kit (Epicentre, Madison, WI, USA). Then, RNA was prepared for sequencing using the ScriptSeq stranded mRNA library prep kit (Illumina). The library was sequenced on a NextSeq500 (Illumina) platform at the University of Queensland, generating 2 × 150 bp paired-end reads with an average insert length of 300 bp.

RNA reads were processed through transcriptM v0.2 (<https://github.com/elfrouin/transcriptM>), including quality trimming using trimmomatic v0.32 [33], PhiX removal using BamM v1.5.0 (<https://github.com/ecogenomics/BamM>), and non-coding RNA removal using sortmerna v2.0 [34]. Processed reads were mapped to the metagenome database assembled from high-coverage reads (described above) by pseudoalignment using kallisto v0.45.0 [35], normalized and analyzed using sleuth v0.30.0 [36] and sleuthALR v0.1.0 [37] with *gyrA* and *gyrB* of ANME-2a as the denominator for compositional normalization [37]; *gyrA* and *gyrB* (DNA gyrase subunits A and B) has been shown to be among the most stable genes in comparative expression analyses [38]. To assess the reliability of abundance estimates by bootstrapping using kallisto [35] and obtain *q*-values (false-discovery rate adjusted *p*-values), a subset of the kallisto results from the day 9 biological triplicates between two conditions were run separately using sleuth v0.30.0 [36] and sleuthALR v0.1.0 [37]. Final expression levels were reported as transcripts per million (TPM) after normalization.

To obtain taxonomy information of the transcripts, the RNA reads were first assembled de novo using Trinity v2.1.1 [39]. Each assembled transcript was then compared to the NCBI refseq proteins as a database using DIAMOND v0.8.11.73 [40] and then the lowest common ancestor of the blast hits was identified using the program blast2lca v0.400 (<https://github.com/emepyc/Blast2lca>). All sequences were assigned to one of eight groups based on their taxonomy string. To obtain metabolic pathway information for the transcripts, assembled transcripts were functionally annotated using the ghostKOALA webserver provided by KEGG (<http://www.kegg.jp/ghostkoala/>), using the "genus_prokaryotes" database. For both taxonomic and metabolic analyses, the sum of the TPM was calculated for each replicate of each condition for each of the taxonomic groups or kegg pathways. The mean and standard deviation was then calculated for each taxonomic group or pathway between the triplicates.

RESULTS

Metabolic rate measurements of methane seep sediment microcosms with different electron acceptors

Anoxic seep sediment slurries in 42 replicated microcosms were incubated under methane and one of four electron acceptor conditions (Supplementary Table 1A): Sulfate, AQDS, AQDS + Sulfate, and None (no electron acceptor added control). Each microcosm quickly resumed AOM activity after electron acceptor addition, as evidenced by the linear increase in concentrations of ¹³C-labeled dissolved inorganic carbon (DIC) produced from ¹³CH₄ (Fig. 1A). Methane oxidation was coupled to sulfate reduction with a stoichiometry close to the expected 1:1 ratio (Fig. 1B). A

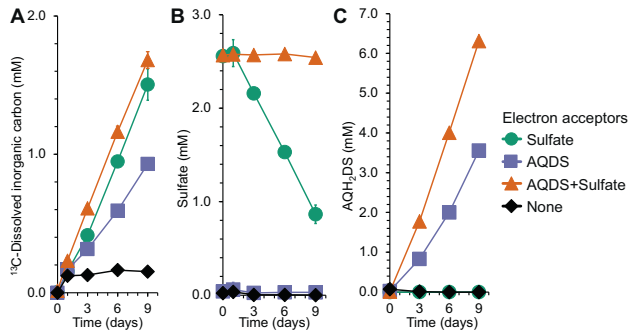


Fig. 1 Metabolic activities of methane-oxidizing consortia in sediment microcosms incubated with methane and different electron acceptors. **A** The oxidation of $^{13}\text{C-CH}_4$ to ^{13}C -dissolved inorganic carbon, **B** the reduction of sulfate, and **C** the reduction of AQDS to AQH₂DS. Error bars represent the standard deviation of biological replicates ($n > 3$, see Supplementary Table 1A), and only the errors larger than the symbols are shown.

negligible amount of sulfate was reduced in the absence of methane (Supplementary Fig. 1), indicating that methane is the dominant electron donor in our microcosms. As reported previously [12], the humic acid analog AQDS was able to serve as an alternative electron acceptor for AOM in the absence of sulfate with a stoichiometry close to the expected 1:4 ratio for $^{13}\text{C-DIC:AQH}_2\text{DS}$ (the reduced form of AQDS; Fig. 1C). The resulting methane oxidation rate coupled to AQDS (0.089 mM CH₄ oxidized per day) in these incubations was 60% of that coupled to sulfate (0.149 mM CH₄ oxidized per day) in parallel microcosms (Fig. 1A), a value that was lower than the previously reported 80% in an independent set of seep sediment experiments [12].

To test the potential influence of sulfate on ANME physiology during AQDS-coupled AOM, we conducted a series of experiments where sulfate was amended at the same electron equivalent concentrations as AQDS (2.5 mM sulfate vs. 10 mM AQDS). Sulfate represents the most oxidized biological sulfur source and does not chemically react with AQDS to produce zero-valent sulfur that was previously shown to be inhibitory to AOM [11]. When AQDS and sulfate were introduced together to sediment in sulfur-free medium, AQDS-coupled AOM was observed (Fig. 1A, C). The methane oxidation rates in the AQDS+Sulfate condition were nearly twofold higher than that with AQDS alone (Fig. 1A, C) and comparable to that recorded during syntrophic sulfate-coupled AOM (0.164 mM CH₄ oxidized per day vs. 0.149 mM CH₄ oxidized per day, respectively; $p = 0.07$) (Fig. 1A). Surprisingly, in the AQDS+Sulfate condition, only AQDS was actively reduced with a stoichiometry close to the expected 1:4 ratio for $^{13}\text{C-DIC:AQH}_2\text{DS}$, but sulfate concentrations remained unchanged over the course of 9 days (Fig. 1B).

Based on these results, a second round of AQDS+Sulfate microcosm experiments were conducted to test the minimal concentration of sulfate required to stimulate AQDS-coupled AOM. We tested six sulfate concentrations ranging between 50 μM and 2.5 mM, equivalent to 560 to 11 times lower than seawater sulfate (28 mM). In the absence of AQDS under conventional sulfate-coupled AOM, sulfate added at concentrations between 50 μM and 2.5 mM were nearly completely consumed within 16 days (down to 4–25 μM with a detection limit of 1 μM) (Fig. 2A). In contrast, with both sulfate and AQDS, sulfate concentrations again remained largely unchanged over this same concentration range (Fig. 2B). Notably, the AQDS reduction rates in these incubations increased with sulfate amendments at all concentrations tested relative to the microcosms with AQDS but without sulfate amendment (Fig. 2C). The stimulatory effect was found to be nearly twofold between 100 μM and 2.5 mM of sulfate amended, with slightly less of an effect on AQDS-coupled AOM with 50 μM sulfate (Fig. 2C).

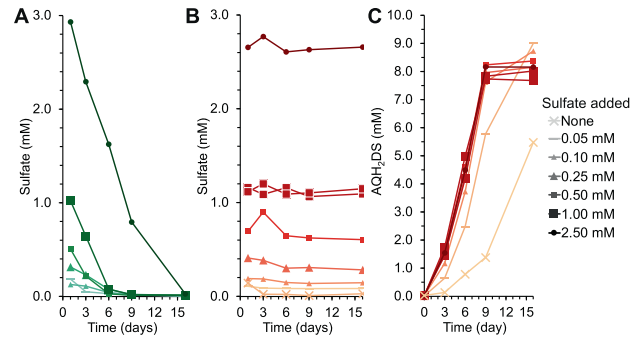


Fig. 2 Sulfate stimulates AQDS-coupled anaerobic oxidation of methane (AOM). **A** In the presence of methane, sulfate was consumed when added as the sole electron acceptor as expected for sulfate-coupled AOM. **B, C** During AQDS-coupled AOM when both AQDS and 50–2500 μM sulfate were added as potential electron acceptors, the concentration of sulfate (**B**) was largely unchanged, but the AQDS reduction rate (**C**) increased with the amendment of as little as 50 μM sulfate. Amendments between 100 μM and 2.5 mM sulfate generated near identical AQDS reduction profiles.

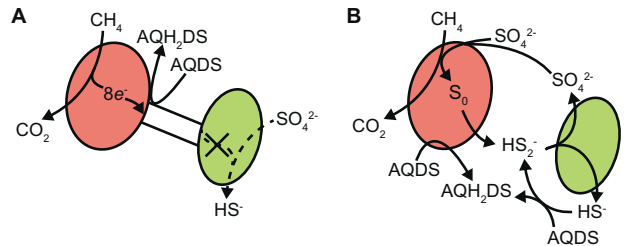


Fig. 3 Schematic showing two hypothetical scenarios of anaerobic oxidation of methane coupled to AQDS as the terminal electron acceptor by ANME-2 and SRB consortia. The ANME-2 cell is represented in red and syntrophic SRB partner is represented in green. **A** In this scenario, ANME oxidize methane and reduce AQDS by extracellular electron transfer [14]. Sulfate stimulates ANME metabolism but is not respired, and the syntrophic SRB are not active. **B** In the alternative scenario, ANME oxidize methane and reduce both AQDS and sulfate. The SRB then disproportionate zero-valent sulfur produced by ANME as hypothesized in Milucka et al. [9]. A cryptic sulfur cycle, with AQDS chemically reacting with sulfide to regenerate zero-valent sulfur is plausible in this scenario, and ANME metabolism increases as a result of the two electron acceptors available. Data from our study is consistent with the extracellular electron transfer scenario shown in **A**, but not the active sulfate respiration and sulfur disproportionation scenario depicted in **B**.

The observed enhancement of AOM with sulfate in the AQDS incubations without appreciable sulfate consumption could be explained by the two main hypotheses about how the AOM syntrophy operates, namely direct interspecies electron transfer [14] or sulfate respiration by ANME-2 [9], with each potentially distinguished based on the activity profiles of ANME and SRB (Fig. 3). Under the direct interspecies electron transfer hypothesis, AQDS serves as a sink for methane-derived electrons that would normally be passed to the sulfate-reducing bacterial partner and it is predicted that only ANME-2 would be active during AQDS-coupled AOM either with or without sulfate amendment (Fig. 3A) [12, 14]. Here, anabolic levels of sulfate could directly stimulate methanotrophy and growth by ANME-2, but their SRB partners remain inactive during this process. Alternatively, in the scenario of sulfate respiration by ANME-2 coupled to zero-valent sulfur disproportionation by the bacterial partner, both ANME and SRB are predicted to be active in the presence of sulfate (Fig. 3B)

[9]. If members of the ANME-2 were capable of actively respiring both sulfate and AQDS in the incubation, then methane oxidation would be stimulated as a result of the availability of two electron acceptors (Fig. 3B). In this scenario, increased AQDS reduction without appreciable net sulfate consumption (Figs. 1 and 2) could be explained by cryptic sulfur cycling involving abiotic reaction of sulfide with AQDS to produce zero-valent sulfur that in turn is disproportionated by SRB to sulfate and sulfide (Fig. 3B). These two scenarios were examined using cell-specific anabolic activity analyses described below.

FISH-nanoSIMS quantification of AOM consortia anabolic activity and cellular sulfur content

Two ANME lineages, namely ANME-2a and ANME-2c, that belong to different archaeal families [41], were shown by amplicon sequencing, metagenomic analysis, and FISH microscopy to be the most abundant methane-oxidizing consortia in our seep sediment microcosm experiments (Supplementary Tables 2 and 3). The ratio of ANME-2a:ANME-2c is estimated to be 1.2:1 by amplicon sequencing (Supplementary Table 2) and is consistent with microscopy observations. To distinguish between the two possible scenarios of sulfate stimulation (Fig. 3), and to examine whether there was any difference in activity between the two distinct ANME-2 families in the different electron acceptor conditions, we conducted FISH-nanoSIMS analyses to measure the anabolic rates (based on ^{15}N -ammonium assimilation [14, 42]) of individual AOM consortia co-occurring in the microcosm experiments after 9 days of incubation (Supplementary Table 4). The FISH-nanoSIMS analysis of cellular ^{15}N enrichment for multiple AOM consortia revealed both the taxonomic identity and anabolic activity at the single-cell level (e.g. McGlynn et al. [14], Fig. 4, Supplementary Fig. 2, and Supplementary Table 4). Two 16S rRNA FISH probes, one newly designed for ANME-2a and one previously developed for ANME-2c (see Materials and methods section), distinguished these two family-level ANME lineages from each other and from their SRB partners [7, 12]. Compared to the no electron acceptor control condition, ANME-2a and ANME-2c were active and had comparable ^{15}N enrichment (ANME-2a consortia mean = 1.55 atom%, s.d. = 0.41%, $n = 5$; ANME-2c consortia mean = 1.61 atom% with values 1.32% and 1.88%, $n = 2$) during sulfate-coupled AOM (Fig. 4). The SRB partners were also anabolically active during sulfate-coupled AOM with higher ^{15}N enrichment (consortia mean = 2.17 atom%, s.d. = 0.87%, $n = 7$) compared to ANME-2 (Fig. 4 and Supplementary Table 5), which is consistent with previous FISH-nanoSIMS results [12, 14]. During AQDS-coupled AOM, SRB partners did not show any anabolic activity as reported previously [12], even in the experimental condition where both AQDS and sulfate were provided (Fig. 4 and Supplementary Tables 4 and 5). This indicates that the SRB partners were not involved in a cryptic sulfur cycle, consuming zero-valent sulfur formed as a result of ANME-2 sulfate respiration (Fig. 3B). Instead, these data are consistent with sulfate directly stimulating ANME-2 during AQDS-coupled AOM (Fig. 3A).

The measured anabolic activity was equivalent between ANME-2a and ANME-2c under conventional sulfate-coupled AOM as well as in the AQDS condition. This pattern was notably different in the microcosms supplied with both AQDS and sulfate, where ANME-2a were more active than ANME-2c. Comparisons of ^{15}N enrichment in ANME-2a revealed a significant ($p = 0.009$) increase in anabolic activity in the AQDS+Sulfate condition (consortia mean = 1.50 atom%, s.d. = 0.32%, $n = 18$) compared to the AQDS condition (consortia mean = 0.57 atom%, s.d. = 0.36%, $n = 17$; Fig. 4; Supplementary Table 4). There was a modest but not statistically significant ($p = 0.078$) increase in the ANME-2c ^{15}N enrichment in the AQDS+Sulfate condition (consortia mean = 1.15 atom%, s.d. = 0.32%, $n = 15$) compared to the AQDS condition (mean = 0.88 atom%, s.d. = 0.38%, $n = 12$; Fig. 4 and Supplementary Table 5). If we assume the higher levels of anabolic

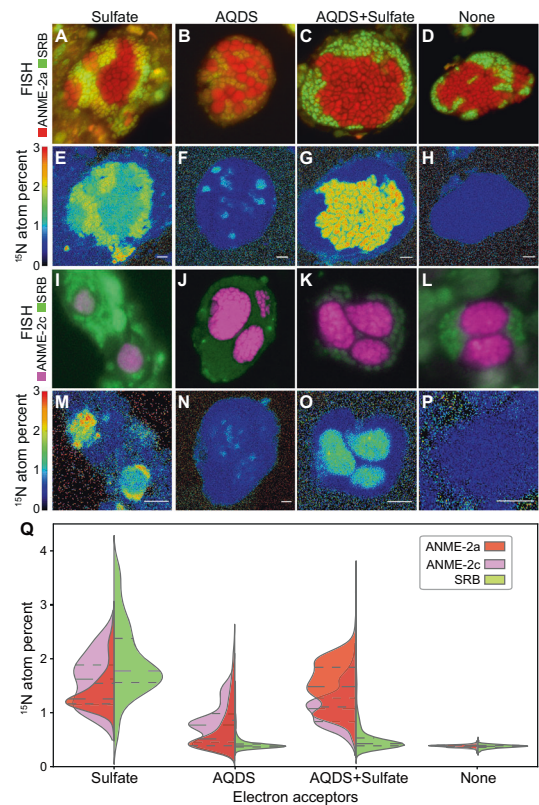


Fig. 4 Paired FISH-nanoSIMS photomicrographs showing anabolic activity for two ANME-2 lineages and their syntrophic bacterial partners with different electron acceptors. A–D and I–L Fluorescence in situ hybridization (FISH) using taxon-specific rRNA-targeted probes distinguish ANME-2a (red in A–D) and ANME-2c (magenta in I, J) from their syntrophic SRB partners (green); **E–H and M–P** Coupled nanometer-scale secondary ion mass spectrometry (nanoSIMS) shows ^{15}N atom percent in regions of interest (ROIs) as cellular anabolic activity proxies for growth in the presence of ^{15}N -ammonium. Scale bars = 3 μm . **Q** Summary of cellular activities in 80 AOM consortia measured using FISH-nanoSIMS after 9 days of incubation. Dashed lines indicate the quartiles of the distributions. The number of aggregates and cell regions of interest for each taxon used in the analyses can be found in Supplementary Tables 4 and 5.

activity documented for ANME-2a consortia are correlated with higher respiration rates (see Supplementary Fig. 3), then these FISH-nanoSIMS results imply that the observed increase in methane oxidation rates in the AQDS+Sulfate condition is primarily attributed to the activity of ANME-2a consortia, with a comparatively minor contribution by ANME-2c.

Previous work examining the physiology of ANME-2 used nanoSIMS to measure $^{32}\text{S}^-$ secondary ions to compare the relative cellular sulfur contents between ANME-2 and their SRB partners in support of sulfate respiration by ANME-2 [9]. Following this work, in tandem with our nanoSIMS measurements of N isotopes, we also measured ^{32}S content in ANME-2a and ANME-2c cells and their SRB partners during sulfate-coupled and AQDS-coupled AOM to compare with the findings of this previous study. We observed comparable sulfur contents between ANME-2 cells and their SRB partners in the same consortium under all experimental conditions tested (Supplementary Fig. 4). Also, the sulfur content in neither ANME-2a nor ANME-2c cells increased with their anabolic activity as measured by ^{15}N -ammonium incorporation (Supplementary Fig. 5). Both of these two observations contrasted with that previously reported during sulfate-coupled AOM [9] and do not support sulfate respiration forming zero-valent sulfur by ANME-2.

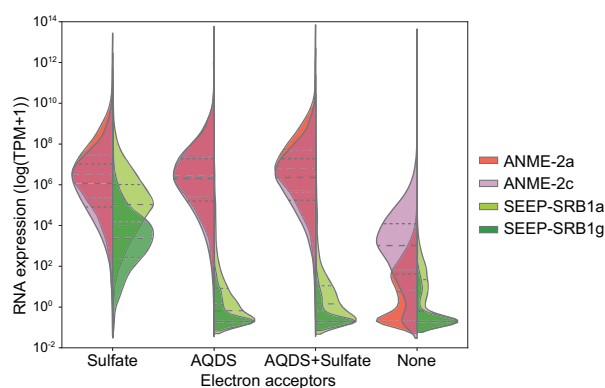


Fig. 5 Gene expression variation of two ANME-2 lineages and two syntrophic sulfate-reducing bacterial lineages with different electron acceptors after 9 days of incubation. RNA expression of ANME-2a, ANME-2c, SEEP-SRB1a, and SEEP-SRB1g was based on their metagenome-assembled genomes and compared using normalized transcript per million reads (TPM) values. Dashed lines indicate the quartiles of the distributions.

Metatranscriptomic analysis of metagenome-assembled genomes to understand ANME-2 response to different electron acceptors

Metatranscriptomic analysis was performed on the sediment microcosms to gain further insight into gene expression changes in ANME-2a and ANME-2c when metabolically decoupled from an active SRB partner, with an emphasis on the potential pathways for sulfate utilization. Metatranscriptome sequencing was conducted on biological triplicates from the same sediment samples as the nanoSIMS analysis after 9 days of incubation, and the results were validated with metatranscriptome samples after 3 days of incubation. This experimental timeframe was chosen to represent ~1–10% of the average ANME-SRB doubling time, reported to range between 3 and 7 months [42–45].

De novo assembly of the transcripts revealed that transcriptional activity in the incubations was largely affiliated with ANME and SRB (Supplementary Text and Supplementary Fig. 6). We reconstructed metagenome-assembled genomes (MAGs) that represent the core genomes of the dominant ANME (ANME-2a and ANME-2c) and SRB lineages (SEEP-SRB1a and SEEP-SRB1g) from the high-coverage metagenomes of the same sediment sample used for the metatranscriptomics analysis (Supplementary Text, Supplementary Table 2, and Supplementary Fig. 7). Transcriptome read mapping to the MAGs revealed that the two most abundant SRB lineages were active in the Sulfate condition, but their transcriptional activities in the AQDS and AQDS+Sulfate conditions dropped to levels comparable to those in the no electron acceptor controls at days 3 and 9 (Fig. 5 and Supplementary Fig. 8). These patterns are consistent with the undetectable ^{15}N -ammonium assimilation with AQDS in the FISH-nanoSIMS analyses at day 9 (Fig. 4). The expression of genes involved in methane and EET pathways in both ANME-2 lineages during sulfate-coupled AOM and AQDS-coupled AOM supported those proposed previously for ANME-2a [14] and were consistent with that of mesophilic ANME-2c [8] (Supplementary Tables 6 and 7).

Through decoupling ANME from their syntrophic SRB partners, we examined the subset of genes that were differentially expressed between sulfate-coupled and AQDS-coupled AOM. We used 2-fold change and q -value (false-discovery rate adjusted p -value) <0.05 as the cutoff for significance and looked for differentially expressed genes that were in common between AQDS and Sulfate conditions and between AQDS+Sulfate and Sulfate conditions. In ANME-2a, 77 genes were significantly upregulated and 37 genes significantly downregulated out of 2012 protein encoding genes. In ANME-2c, 54 genes were significantly upregulated, while no genes were

significantly downregulated out of 1976 protein encoding genes (Fig. 6A and Supplementary Table 8). Of this set of differentially expressed genes, 63% of ANME-2a and 48% in ANME-2c could be annotated based on homology to known proteins or functions (i.e. not hypothetical or uncharacterized). In ANME-2a and ANME-2c, several ATP-binding cassette (ABC) family transporters were significantly upregulated during AQDS-coupled AOM (7 genes in 3 gene clusters in ANME-2a, 7 genes in 3 gene clusters in ANME-2c). Most lacked information about the potential substrate, with a subset identified as putatively linked to molybdate/tungstate or osmoprotectant transport. Also significantly upregulated in the presence of AQDS in both ANME-2 families were genes encoding a sodium: proton antiporter (Mrp). In ANME-2c, genes encoding for molybdopterin synthase and nitrogenase subunits (nifD and nifH) were significantly upregulated. Of the genes that were significantly downregulated during AQDS-coupled AOM compared to sulfate-coupled AOM, ANME-2a showed a decrease in expression of those genes encoding proteins involved in methane oxidation (Fmd, Ftr, Mtd, Mer, Mch, Mtr) and energy conservation (Fpo), and several heme-containing proteins including the membrane-spanning cytochrome *b* and adjacent multiheme cytochrome *c* that were hypothesized to be important for EET [14, 46] (Fig. 6A and Supplementary Table 8).

To further investigate the observed differential stimulatory effect of sulfate on ANME-2a relative to ANME-2c lineages during AQDS-coupled AOM, we searched for differentially expressed genes between AQDS+Sulfate and AQDS conditions. This analysis revealed that ANME-2a had more differentially expressed genes (78 genes significantly upregulated and 2 genes significantly downregulated) compared with ANME-2c (10 genes significantly upregulated and 9 genes significantly downregulated; Supplementary Table 9) in line with the FISH-nanoSIMS results. We specifically searched for genes associated with sulfur metabolism [11]. Neither the ANME-2a nor ANME-2c MAGs contained genes encoding Sat and CysDN proteins required for sulfate activation, consistent with previous reports [8, 11, 47]. In ANME-2a, there were six upregulated genes ($q < 0.05$), that encode proteins predicted to be involved in sulfur assimilation but most were upregulated <2 fold (1 fold indicates no upregulation) and did not meet our ‘significance’ criteria. We mention them here as they are potentially linked to the stimulatory response observed in the AQDS+Sulfate condition. In the order of lowest to highest differential expression, these included cysteine desulfurase (1.1 fold), assimilatory APS reductase (1.2 fold), F_{420} -dependent sulfite reductase (Fsr) (1.3 fold), PAPS reductase (1.4 fold), and assimilatory-type low-spin sulfite reductase (alSir) (2.1 fold) (Fig. 6B and Supplementary Table 6). In ANME-2c, three genes encode proteins that may be involved in sulfur assimilation; all were similarly expressed between AQDS+Sulfate and AQDS conditions: adenylylsulfate kinase (1.1 fold), alSir (1.0 fold), and Fsr (1.0 fold) (Fig. 6B and Supplementary Table 7). Beyond this suite of genes, we did not observe other candidates that may be linked to sulfur anabolism (or sulfate respiration) in ANME-2a or ANME-2c from our genomic and transcriptomic data that provides additional insight into how sulfate is specifically used by either ANME-2a or ANME-2c. We note that 37–52% of the genes differentially expressed in ANME-2a and ANME-2c are currently uncharacterized and it is possible that additional insights will be gained through future functional analyses.

DISCUSSION

Syntrophic partnerships between diverse ANME and SRB lineages in methane seeps play an important role in ocean methane cycling, but we still lack fundamental details about their physiology, syntrophic mechanisms, and potential ecological differences between the major ANME lineages. In this study, we leveraged the use of an alternative electron acceptor, AQDS, a

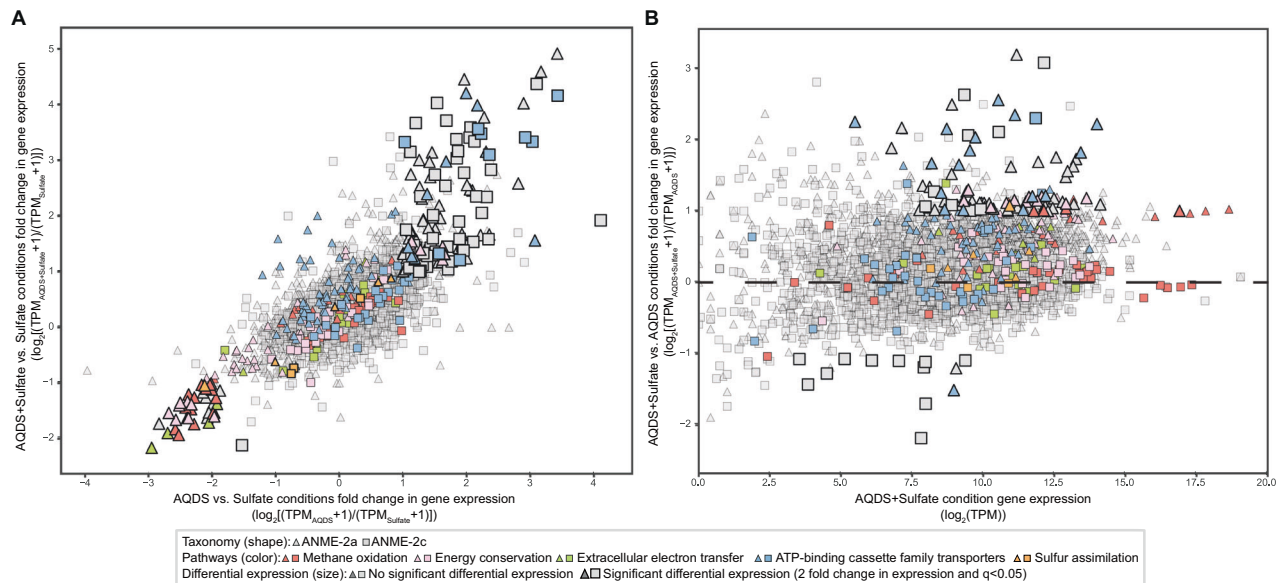


Fig. 6 Differential expression of key pathways by two ANME-2 lineages from comparative metatranscriptomics. A Differential gene expression after decoupling ANME-2 lineages from their syntrophic SRB partners using AQDS. In this comparison of the fold change in gene expression between the AQDS and Sulfate conditions (x-axis) and between AQDS + Sulfate and Sulfate conditions (y-axis), the upper right quadrant represents upregulated genes and the lower left quadrant represents downregulated genes during AQDS-coupled AOM. **B** Transcriptional response of ANME-2 lineages with and without sulfate amendment during AQDS-coupled AOM. In this comparison of gene expression in the AQDS + Sulfate condition (x-axis) and the fold change in gene expression between AQDS + Sulfate and AQDS conditions (y-axis), the majority of the sulfur anabolism genes were not significantly upregulated with sulfate amendment. The only significantly upregulated sulfur anabolism gene was assimilatory-type low-spin sulfite reductase in ANME-2a. Both panels used the mean of gene expression values from triplicate samples in each experimental condition after 9 days of incubation.

chemical analog for humic substances, to decouple the activity of ANME from their SRB partners in sediment microcosm experiments. Our results on two different ANME-2 families, ANME-2a and ANME-2c, addressed outstanding questions about AOM syntrophy and ecophysiological variation among ANME-2 lineages. By targeting our analysis on the anabolic and catabolic response of these uncultured methanotrophic archaea independent of active syntrophic SRB partners with and without sulfate amendment, we sought to test the capability of methanotrophic ANME-2 to reduce sulfate following the earlier hypothesized mechanism outlined in [9] where methane oxidation directly coupled sulfate reduction by ANME-2 was proposed. As our methane seep sediment microcosm experiments contained a nearly equal abundance of ANME-2a and ANME-2c consortia, we additionally analyzed potential differences in the response of these two coexisting ANME-2 families under the different electron acceptor conditions using single-cell resolved FISH-nanoSIMS analyses and comparative transcriptomics.

Our findings indicate that ANME-2 couple methane oxidation to EET [13, 14, 48] rather than sulfate respiration [9]. The growing number of ANME genomes have lacked evidence of homologs for the dissimilatory sulfate reduction pathway [8, 11, 47], but it is difficult to completely rule out the possibility of an unknown mechanism for ANME sulfate respiration. ANME-2a and ANME-2c were shown to be anabolically and catabolically active without sulfate respiration (Figs. 1, 2, 4, and 5) [12], indicating the coupling AOM to dissimilatory sulfate reduction and production of zero-valent sulfur as a metabolic product is not essential, even by the same ANME lineages studied previously [9, 10]. FISH-nanoSIMS analysis revealed that the cellular sulfur content of ANME cells was not elevated above that of their SRB partner cells (Supplementary Fig. 4) and it did not correlate with anabolic activity (Supplementary Fig. 5). This cell-specific sulfur data differs from the previous study that proposed zero-valent sulfur syntrophy and active sulfate respiration by ANME [9], in which ANME cells had elevated cellular sulfur relative to SRB and ANME cellular sulfur content and anabolic activity were positively correlated. Further, while

autotrophic growth of the SEEP-SRB1a partner was initially reported after amendment with zero-valent sulfur [9], long-term growth of the syntrophic SEEP-SRB1a, SEEP-SRB2, and HotSeep-1 partners of ANME-1 and ANME-2 on zero-valent sulfur have proven unsuccessful [6, 11]. Our study examined the same ANME-2 lineages as the study that proposed sulfate respiration by ANME [9], and the results are instead consistent with these ANME-2 lineages capable of EET and direct interspecies electron transfer [13, 14, 48] that facilitates the disposal of methane-derived electrons to either their syntrophic SRB partner or artificial electron acceptors such as AQDS. Engaging in direct interspecies electron transfer could be a general trait for AOM syntrophy, as a growing number of studies report the identification [14, 48], expression (Supplementary Tables 6 and 7) [8, 49, 50] and detection [8, 14] of a multiheme cytochrome *c* based EET conduit in different ANME lineages.

Coexisting ANME-2a and ANME-2c consortia responded differently to sulfate amendment, as revealed by metabolic rate measurements in tandem with FISH-nanoSIMS single-cell analysis of anabolic activity and metatranscriptomics. When decoupled from their syntrophic SRB partners, ANME-2a cells had significantly higher anabolic activities than ANME-2c in response to sulfate amendment during AQDS-coupled AOM. In marine environments, ANME lineages have been observed to niche separate based on temperature, sediment depth, sediment surface community, and substrate concentrations including sulfate [30, 51–54]. Experimentally, ANME-1 and ANME-2 growth was different depending on the condition [55, 56], and SRB partners could be differentially active based on the available nitrogen species [57]. Our results imply that ANME-2a cells were primarily responsible for the observed stimulatory effect with sulfate (Fig. 4): There are several possible explanations for this sulfate stimulation. Sulfate may provide ANME-2a with a required source of anabolic sulfur during AQDS-coupled AOM. While the sulfate concentration remained largely unchanged over the course of our experiments (Figs. 1B and 2B), we estimate that ANME growth would only require 0.25 μM of

sulfate over 9 days, given that 1.68 mM CH₄ was oxidized in the AQDS+Sulfate condition (Fig. 1A) and assuming that ANME could assimilate sulfate with an assimilation efficiency of 0.6% [58] and a cellular carbon:sulfur ratio of 40:1 [59]. Future experiments with higher sensitivity or isotope label would be needed to determine and track sulfate consumption and incorporation. However, our ANME-2a and ANME-2c MAGs are consistent with the previous study that showed these lineages do not encode a full assimilatory sulfate reduction pathway, in particular missing ATP sulfurylases (Sat or CysDN) for sulfate activation [11]. While members of the ANME-2a and ANME-2c both encode homologs to downstream steps in the assimilatory sulfate reduction pathway (Supplementary Tables 6 and 7), the lack of a mechanism to form adenosine 5'-phosphosulfate indicates that sulfate stimulation by ANME-2a is not occurring through canonical sulfate assimilation. Alternatively, sulfate could be involved in ANME-2 anabolism without being reduced. For example, it is possible that sulfate is used by ANME-2 to produce a redox active compound, like thioquinoxalinol sulfate identified in ANME-1a consortia [17]. When a sulfate ester group is added to thioquinoxalinol, the resulting thioquinoxalinol sulfate becomes more water soluble and therefore more readily available for redox shuttling [17]. If a similar redox active sulfur-containing molecule is produced by ANME-2 and used for electron shuttling, this could lead to enhanced rates of AQDS-coupled AOM and anabolic activity above that observed from EET alone. This type of combined electron transport has been observed in model EET bacteria such as *Shewanella oneidensis* with flavins [60–62]. The biosynthetic pathway for thioquinone is currently unknown and follow up research is needed to determine whether this is a common metabolite among all ANME lineages and its specific role in their metabolism.

AQDS and related compounds have been reported to inhibit microorganisms including sulfate-reducing bacteria [63–67], likely due to their structural similarity to redox active antibiotics once transported into the cell cytoplasm [68]. Some bacteria and archaea on the other hand, including members of the *Methanosarcinales*, not only tolerate AQDS but directly respire this redox active humic analog [69–71]. The underlying biochemical pathways used by ANME-2 to tolerate and reduce AQDS are unknown, but insights may be drawn from known AQDS reduction mechanisms in other microorganisms. For example, in the gram negative bacterium *Shewanella oneidensis*, the TolC component of the ArcAB-TolC efflux pump is essential for preventing AQDS toxicity [68]. As part of the tripartite efflux pump, TolC located in the outer membrane may form complexes with different periplasmic and cytoplasmic membrane components in the resistance-nodulation-division (RND), major facilitator superfamily (MFS), or ATP-binding cassette (ABC) family transporters [72]. In line with these findings, multiple ABC transporter operons were significantly upregulated in both ANME-2a and ANME-2c in all experimental conditions containing AQDS (Supplementary Tables 6 and 7). One of the upregulated ABC transporter operons in ANME-2a (IMG gene ID 2842053615–2842053619) and ANME-2c (IMG gene ID 2842579012–2842579013) is homologous to the MacAB-TolC efflux pump for secretion of enterotoxin in *Escherichia coli* [73], and could be a promising candidate in future study for the role in AQDS efflux. None of the genes predicted to be involved in EET in ANME-2a and ANME-2c were significantly upregulated when comparing metatranscriptomics during AQDS-coupled AOM to sulfate-coupled AOM, and therefore did not reveal an obvious AQDS reduction pathway. However, the lack of an observed change in transcriptional response in putative EET genes in ANME is not unexpected in light of studies on the model electrogenic bacterium *Geobacter sulfurreducens*, where genes essential for EET were constitutively expressed under conditions of electrode growth and fumarate reduction [74]. *Methanosarcina acetivorans*, a methanogenic archaeon belonging to the same order as ANME-2, is capable of growth using AQDS as the terminal

electron acceptor. Transcriptomic and genetic analyses have linked AQDS reduction in *M. acetivorans* to the multiheme *c* type cytochrome Mmca, indicating this may be a potential candidate for AQDS reduction in ANME-2 [71]. Genomic analyses identified a Mmca homolog in ANME-2a but not ANME-2c. As observed with the other putative EET genes, this Mmca was not upregulated during AQDS-coupled AOM compared to sulfate-coupled AOM in our experiments.

Methanotrophic ANME lineages are highly diverse and polyphyletic [1], encompassing two orders and four families within the *Halobacteriota* phylum [1, 41]. This taxonomic diversity translates to differences in their ecology and physiological responses. By measuring both metabolic and anabolic activities of two distinct ANME families (ANME-2a and ANME-2c), we identified differences in the degree to which sulfate stimulates the anabolic activity of these archaea in the presence of AQDS. ANME-2a showed a significantly higher anabolic activity response relative to ANME-2c in the experimental condition containing both AQDS and sulfate. Transcriptomics further revealed differential expression of metabolic and energy conservation genes in ANME-2a when decoupled from their syntrophic bacterial partner, perhaps associated with fine tuning their metabolism in response to AQDS as the terminal electron acceptor and its redox potential. Changes in the expression of central metabolism genes have also been previously reported for syntrophic co-cultures of *Desulfovibrio vulgaris* and *Methanococcus maripalutis* [75, 76] and for phototrophic consortia of "*Chlorobium chlorochromatii*" CaD3 and betaproteobacteria [77], when decoupled from their respective syntrophic partners, suggesting this may be a generalized response to a syntrophic lifestyle. How sulfate is specifically used by ANME-2a resulting in enhanced methane oxidation and biosynthetic activity remains unknown, however, elucidating the underlying biochemical mechanisms has relevance not only for advancing our understanding of ANME physiology, but also for related methanogenic archaea. While members of the ANME-2 archaea have yet to be obtained in pure culture, these culture-independent single-cell measurements of their anabolic activity, combined with comparative metatranscriptomics during sulfate-coupled and AQDS-coupled AOM provide new insights into ANME-2 metabolic requirements. This in turn suggests new cultivation strategies for these environmentally and biotechnologically important archaea that may ultimately yield axenic strains for detailed physiological and biochemical analysis.

DISCLAIMER

This report was prepared as an account of work sponsored by an agency of the United States Government. Neither the United States Government nor any agency thereof, nor any of their employees, makes any warranty, express or implied, or assumes any legal liability or responsibility for the accuracy, completeness, or usefulness of any information, apparatus, product, or process disclosed, or represents that its use would not infringe privately owned rights. Reference herein to any specific commercial product, process, or service by trade name, trademark, manufacturer, or otherwise does not necessarily constitute or imply its endorsement, recommendation, or favoring by the United States Government or any agency thereof. The views and opinions of authors expressed herein do not necessarily state or reflect those of the United States Government or any agency thereof.

DATA AVAILABILITY

The high-coverage metagenomic assembly and metagenome-assembled genomes (MAGs) from this study can be found in Joint Genome Institute Genome Online Database under Study ID Gs0135232. Also, the metagenomic reads, transcriptomic reads and MAGs can be found under National Center for Biotechnology Information

BioProject IDs PRJNA431796 and PRJNA576751. Database IDs for each MAG can be found in Supplementary Table 3.

REFERENCES

- Knittel K, Boetius A. Anaerobic oxidation of methane: progress with an unknown process. *Annu Rev Microbiol.* 2009;63:311–34.
- Reeburgh WS. Oceanic methane biogeochemistry. *Chem Rev.* 2007;107:486–513.
- Hatzenpichler R, Connon SA, Goudeau D, Malmstrom RR, Woyke T, Orphan VJ. Visualizing in situ translational activity for identifying and sorting slow-growing archaeal–bacterial consortia. *Proc Natl Acad Sci USA.* 2016;113:E4069–E4078.
- Skenneron CT, Chourey K, Iyer R, Hettich RL, Tyson GW, Orphan VJ. Methane-fueled syntrophy through extracellular electron transfer: uncovering the genomic traits conserved within diverse bacterial partners of anaerobic methanotrophic archaea. *mBio.* 2017;8:e00530–e00517.
- Orphan VJ, House CH, Hinrichs K-U, McKeegan KD, DeLong EF. Multiple archaeal groups mediate methane oxidation in anoxic cold seep sediments. *Proc Natl Acad Sci USA.* 2002;99:7663–8.
- Wegener G, Krukenberg V, Ruff SE, Kellermann MY, Knittel K. Metabolic capabilities of microorganisms involved in and associated with the anaerobic oxidation of methane. *Front Microbiol.* 2016;7:869.
- Metcalfe KS, Murali R, Mullin SW, Connon SA, Orphan VJ. Experimentally-validated correlation analysis reveals new anaerobic methane oxidation partnerships with consortium-level heterogeneity in diazotrophy. *ISME J.* 2020;15:377–96.
- Krukenberg V, Riedel D, Gruber-Vodicka HR, Buttigieg PL, Tegetmeyer HE, Boetius A, et al. Gene expression and ultrastructure of meso- and thermophilic methanotrophic consortia. *Environ Microbiol.* 2018;20:1651–6.
- Milucka J, Ferdelman TG, Polerecky L, Franzke D, Wegener G, Schmid M, et al. Zero-valent sulphur is a key intermediate in marine methane oxidation. *Nature.* 2012;491:541–6.
- Schreiber L, Holler T, Knittel K, Meyerdierks A, Amann R. Identification of the dominant sulfate-reducing bacterial partner of anaerobic methanotrophs of the ANME-2 clade. *Environ Microbiol.* 2010;12:2327–40.
- Yu H, Susanti D, McGlynn SE, Skenneron CT, Chourey K, Iyer R, et al. Comparative genomics and proteomic analysis of assimilatory sulfate reduction pathways in anaerobic methanotrophic archaea. *Front Microbiol.* 2018;9:2917
- Scheller S, Yu H, Chadwick GL, McGlynn SE, Orphan VJ. Artificial electron acceptors decouple archaeal methane oxidation from sulfate reduction. *Science.* 2016;351:703–7.
- Wegener G, Krukenberg V, Riedel D, Tegetmeyer HE, Boetius A. Intercellular wiring enables electron transfer between methanotrophic archaea and bacteria. *Nature.* 2015;526:587–90.
- McGlynn SE, Chadwick GL, Kempes CP, Orphan VJ. Single cell activity reveals direct electron transfer in methanotrophic consortia. *Nature.* 2015;526:531–5.
- Liu Y, Beer LL, Whitman WB. Sulfur metabolism in archaea reveals novel processes. *Environ Microbiol.* 2012;14:2632–44.
- Perona JJ, Rauch BJ, Driggers CM. Sulfur assimilation and trafficking in methanogens. In: Rampelotto PH, editor. *Molecular Mechanisms of Microbial Evolution.* Cham: Springer International Publishing; 2018. p. 371–408.
- White RH, Allen KD, Wegener G. Identification of a redox active thioquinoxalinal sulfate compound produced by an anaerobic methane-oxidizing microbial consortium. *ACS Omega.* 2019;4:22613–22.
- Cline JD. Spectrophotometric determination of hydrogen sulfide in natural waters. *Limnol Oceanogr.* 1969;14:454–8.
- Caporaso JG, Kuczynski J, Stombaugh J, Bittinger K, Bushman FD, Costello EK, et al. QIIME allows analysis of high-throughput community sequencing data. *Nat Methods.* 2010;7:335–6.
- Edgar RC. Search and clustering orders of magnitude faster than BLAST. *Bioinformatics.* 2010;26:2460–1.
- Quast C, Pruesse E, Yilmaz P, Gerken J, Schweer T, Yarza P, et al. The SILVA ribosomal RNA gene database project: improved data processing and web-based tools. *Nucleic Acids Res.* 2013;41:D590–6.
- Mason OU, Case DH, Naehr TH, Lee RW, Thomas RB, Bailey JV, et al. Comparison of archaeal and bacterial diversity in methane seep carbonate nodules and host sediments, Eel River Basin and Hydrate Ridge, USA. *Microb Ecol.* 2015;70:766–84.
- Laczny CC, Sternal T, Plugaru V, Gawron P, Atashpendar A, Margossian HH, et al. VizBin - an application for reference-independent visualization and human-augmented binning of metagenomic data. *Microbiome.* 2015;3:1.
- Parks DH, Imelfort M, Skenneron CT, Hugenholtz P, Tyson GW. CheckM: assessing the quality of microbial genomes recovered from isolates, single cells, and metagenomes. *Genome Res.* 2015;25:1043–55.
- Hyatt D, Chen G-L, LoCasio PF, Land ML, Larimer FW, Hauser LJ. Prodigal: prokaryotic gene recognition and translation initiation site identification. *BMC Bioinform.* 2010;11:119.
- Chen I-MA, Chu K, Palaniappan K, Pillay M, Ratner A, Huang J, et al. IMG/M v.5.0: an integrated data management and comparative analysis system for microbial genomes and microbiomes. *Nucleic Acids Res.* 2019;47:D666–D677.
- Agarwala R, Barrett T, Beck J, Benson DA, Bollin C, Bolton E, et al. Database resources of the National Center for Biotechnology Information. *Nucleic Acids Res.* 2018;46:D8–D13.
- Saier MH, Reddy VS, Tsu BV, Ahmed MS, Li C, Moreno-Hagelsieb G. The Transporter Classification Database (TCDB): recent advances. *Nucleic Acids Res.* 2016;44:D372–D379.
- Li H, Durbin R. Fast and accurate short read alignment with Burrows–Wheeler transform. *Bioinformatics.* 2009;25:1754–60.
- Knittel K, Losekann T, Boetius A, Kort R, Amann R. Diversity and distribution of methanotrophic archaea at cold seeps. *Appl Environ Microbiol.* 2005;71:467–79.
- Manz W, Eisenbrecher M, Neu TR, Szewzyk U. Abundance and spatial organization of Gram-negative sulfate-reducing bacteria in activated sludge investigated by in situ probing with specific 16S rRNA targeted oligonucleotides. *FEMS Microbiol Ecol.* 1998;25:43–61.
- Polerecky L, Adam B, Milucka J, Musat N, Vagner T, Kuypers MMM. Look@NanoSIMS – a tool for the analysis of nanoSIMS data in environmental microbiology. *Environ Microbiol.* 2012;14:1009–23.
- Bolger AM, Lohse M, Usadel B. Trimmomatic: a flexible trimmer for Illumina sequence data. *Bioinformatics.* 2014;30:2114–20.
- Kopylova E, Noe L, Touzet H. SortMeRNA: fast and accurate filtering of ribosomal RNAs in metatranscriptomic data. *Bioinformatics.* 2012;28:3211–7.
- Bray NL, Pimentel H, Melsted P, Pachter L. Near-optimal probabilistic RNA-seq quantification. *Nat Biotechnol.* 2016;34:525–7.
- Pimentel H, Bray NL, Puente S, Melsted P, Pachter L. Differential analysis of RNA-seq incorporating quantification uncertainty. *Nat Methods.* 2017;14:687–90.
- McGee WA, Pimentel H, Pachter L, Wu JY. Compositional Data Analysis is necessary for simulating and analyzing RNA-Seq data. *bioRxiv* 2019;564955.
- Rocha DJP, Santos CS, Pacheco LGC. Bacterial reference genes for gene expression studies by RT-qPCR: survey and analysis. *Antonie van Leeuwenhoek.* 2015;108:685–93.
- Grabherr MG, Haas BJ, Yassour M, Levin JZ, Thompson DA, Amit I, et al. Full-length transcriptome assembly from RNA-Seq data without a reference genome. *Nat Biotechnol.* 2011;29:644–52.
- Buchfink B, Xie C, Huson DH. Fast and sensitive protein alignment using DIAMOND. *Nat Methods.* 2015;12:59–60.
- Rinke C, Chuvochina M, Mussig AJ, Chaumeil P-A, Davin AA, Waite DW, et al. A standardized archaeal taxonomy for the Genome Taxonomy Database. *Nat Microbiol.* 2021;6:946–59.
- Orphan VJ, Turk KA, Green AM, House CH. Patterns of ¹⁵N assimilation and growth of methanotrophic ANME-2 archaea and sulfate-reducing bacteria within structured syntrophic consortia revealed by FISH-SIMS. *Environ Microbiol.* 2009;11:1777–91.
- Girguis PR, Cozen AE, DeLong EF. Growth and population dynamics of anaerobic methane-oxidizing archaea and sulfate-reducing bacteria in a continuous-flow bioreactor. *Appl Environ Microbiol.* 2005;71:3725–33.
- Nauhaus K, Albrecht M, Elvert M, Boetius A, Widdel F. In vitro cell growth of marine archaeal-bacterial consortia during anaerobic oxidation of methane with sulfate. *Environ Microbiol.* 2007;9:187–96.
- Meulepas RJW, Jagersma CG, Khadem AF, Buisman CJN, Stams AJM, Lens PNL. Effect of environmental conditions on sulfate reduction with methane as electron donor by an Eckernförde Bay enrichment. *Environ Sci Technol.* 2009;43:6553–9.
- McGlynn SE. Energy metabolism during anaerobic methane oxidation in ANME archaea. *Microbes Environ.* 2017;32:5–13.
- Wang F-P, Zhang Y, Chen Y, He Y, Qi J, Hinrichs K-U, et al. Methanotrophic archaea possessing diverging methane-oxidizing and electron-transporting pathways. *ISME J.* 2014;8:1069–78.
- Meyerdierks A, Kube M, Kostadinov I, Teeling H, Glöckner FO, Reinhardt R, et al. Metagenome and mRNA expression analyses of anaerobic methanotrophic archaea of the ANME-1 group. *Environ Microbiol.* 2010;12:422–39.
- Cai C, Leu AO, Xie G-J, Guo J, Feng Y, Zhao J-X, et al. A methanotrophic archaeon couples anaerobic oxidation of methane to Fe(III) reduction. *ISME J.* 2018;1:285.
- Leu AO, Cai C, McIlroy SJ, Southam G, Orphan VJ, Yuan Z, et al. Anaerobic methane oxidation coupled to manganese reduction by members of the Methanoperedenaceae. *ISME J.* 2020;14:1030–41.
- Yanagawa K, Sunamura M, Lever MA, Morono Y, Hiruta A, Ishizaki O, et al. Niche separation of methanotrophic archaea (ANME-1 and-2) in methane-seep sediments of the eastern Japan Sea offshore Joetsu. *Geomicrobiol J.* 2011;28:118–29.

52. Biddle JF, Cardman Z, Mendlovitz H, Albert DB, Lloyd KG, Boetius A, et al. Anaerobic oxidation of methane at different temperature regimes in Guaymas Basin hydrothermal sediments. *ISME J.* 2012;6:1018–31.
53. Holler T, Widdel F, Knittel K, Amann R, Kellermann MY, Hinrichs K-U, et al. Thermophilic anaerobic oxidation of methane by marine microbial consortia. *ISME J.* 2011;5:1946–56.
54. Roalkvam I, Jørgensen SL, Chen Y, Stokke R, Dahle H, Hocking WP, et al. New insight into stratification of anaerobic methanotrophs in cold seep sediments. *FEMS Microbiol Ecol.* 2011;78:233–43.
55. Timmers PHA, Widjaja-Greefkes HCA, Ramiro-García J, Plugge CM, Stams AJM. Growth and activity of ANME clades with different sulfate and sulfide concentrations in the presence of methane. *Front Microbiol.* 2015;6:988.
56. Nauhaus K, Treude T, Boetius A, Krüger M. Environmental regulation of the anaerobic oxidation of methane: a comparison of ANME-I and ANME-II communities. *Environ Microbiol.* 2005;7:98–106.
57. Green-Saxena A, Dekas AE, Dalleska NF, Orphan VJ. Nitrate-based niche differentiation by distinct sulfate-reducing bacteria involved in the anaerobic oxidation of methane. *ISME J.* 2014;8:150–63.
58. Wegener G, Niemann H, Elvert M, Hinrichs K-U, Boetius A. Assimilation of methane and inorganic carbon by microbial communities mediating the anaerobic oxidation of methane. *Environ Microbiol.* 2008;10:2287–98.
59. Scherer P, Lippert H, Wolff G. Composition of the major elements and trace elements of 10 methanogenic bacteria determined by inductively coupled plasma emission spectrometry. *Biol Trace Elem Res.* 1983;5:149–63.
60. Marsili E, Baron DB, Shikhare ID, Coursolle D, Gralnick JA, Bond DR. *Shewanella* secretes flavins that mediate extracellular electron transfer. *Proc Natl Acad Sci USA.* 2008;105:3968–73.
61. Kotloski NJ, Gralnick JA. Flavin electron shuttles dominate extracellular electron transfer by *Shewanella oneidensis*. *mBio* 2013;4:e00553-12.
62. Mevers E, Su L, Pishchany G, Baruch M, Cornejo J, Hobert E, et al. An elusive electron shuttle from a facultative anaerobe. *eLife.* 2019;8:e48054.
63. Weimer PJ, Odom JM, Cooling FB, Anderson AG. Anthraquinones as inhibitors of sulfide production from sulfate-reducing bacteria. US Patent 5385842. 1995.
64. Wang X, Cheng X, Ren Y, Xu G, Tang J. Humic analog AQDS can act as a selective inhibitor to enable anoxygenic photosynthetic bacteria to outcompete sulfate-reducing bacteria under microaerobic conditions. *J Chem Technol Biotechnol.* 2016;91:2103–10.
65. Lee YH, Pavlostathis SG. Decolorization and toxicity of reactive anthraquinone textile dyes under methanogenic conditions. *Water Res.* 2004;38:1838–52.
66. Wu Y-W, Ouyang J, Xiao X-H, Gao W-Y, Liu Y. Antimicrobial properties and toxicity of anthraquinones by microcalorimetric bioassay. *Chin J Chem.* 2006;24:45–50.
67. Novotný Č, Dias N, Kapanen A, Malachová K, Váňdřovcová M, Itävaara M, et al. Comparative use of bacterial, algal and protozoan tests to study toxicity of azo- and anthraquinone dyes. *Chemosphere.* 2006;63:1436–42.
68. Shyu JBH, Lies DP, Newman DK. Protective role of toIC in efflux of the electron shuttle anthraquinone-2,6-disulfonate. *J Bacteriol.* 2002;184:1806–10.
69. Lovley DR, Coates JD, Blunt-Harris EL, Phillips EJP, Woodward JC. Humic substances as electron acceptors for microbial respiration. *Nature.* 1996;382:445–8.
70. Newman DK, Kolter R. A role for excreted quinones in extracellular electron transfer. *Nature.* 2000;405:94–7.
71. Holmes DE, Ueki T, Tang H-Y, Zhou J, Smith JA, Chaput G, et al. A membrane-bound cytochrome enables *Methanosarcina acetivorans* to conserve energy from extracellular electron transfer. *mBio.* 2019;10:e00789–19.
72. Neuberger A, Du D, Luisi BF. Structure and mechanism of bacterial tripartite efflux pumps. *Res Microbiol.* 2018;169:401–13.
73. Crow A, Greene NP, Kaplan E, Koronakis V. Structure and mechanotransmission mechanism of the MacB ABC transporter superfamily. *Proc Natl Acad Sci USA.* 2017;114:12572–7.
74. Jiménez-Otero F, Chan CH, Bond DR. Identification of different putative outer membrane electron conduits necessary for Fe (III) citrate, Fe (III) oxide, Mn (IV) oxide, or electrode reduction by *Geobacter sulfurreducens*. *J Bacteriol.* 2018;200:3061.
75. Plugge CM, Scholten JCM, Culley DE, Nie L, Brockman FJ, Zhang W. Global transcriptomics analysis of the *Desulfovibrio vulgaris* change from syntrophic growth with *Methanosarcina barkeri* to sulfidogenic metabolism. *Microbiology.* 2010;156:2746–56.
76. Walker CB, He Z, Yang ZK, Ringbauer JAJ, He Q, Zhou J, et al. The electron transfer system of syntrophically grown *Desulfovibrio vulgaris*. *J Bacteriol.* 2009;191:5793–801.
77. Wenter R, Hütz K, Dibbern D, Li T, Reisinger V, Plöschner M, et al. Expression-based identification of genetic determinants of the bacterial symbiosis '*Chlorochromatium aggregatum*'. *Environ Microbiol.* 2010;12:2259–76.

ACKNOWLEDGEMENTS

We thank our colleagues, facilities managers, and staff at Caltech: Stephanie Connon for assistance with iTAG sample preparation; Ranjani Murali for assistance with sulfate-reducing bacteria phylogeny; Haley Sapers for comments on the manuscript; Nathan Dalleska for assistance with ion chromatography at the Environmental Analysis Center; Yunbin Guan for assistance with nanoSIMS analyses at the Microanalysis Center in the Division of Geological and Planetary Sciences; Fan Gao for valuable discussions on transcriptome analysis at Bioinformatics Resource Center in the Beckman Institute; David Vander Velde for nuclear magnetic resonance analysis at the Liquid NMR Facility in the Division of Chemistry and Chemical Engineering. We also thank Margaret Butler at University of Queensland for assistance with RNA sample preparation and sequencing. We further acknowledge the support from the Monterey Bay Aquarium Research Institute (MBARI) and the pilots and crew of the R/W *Western Flyer* and ROV Doc Ricketts who supported the field expedition and sample collection. Special thanks to three anonymous reviewers for their constructive comments on the manuscript. This work was supported by the United States Department of Energy's Office of Science Biological and Environmental Research Program (DE-SC0016469 and DE-SC0020373), Caltech's Center for Environmental Microbial Interactions (CEMI), and the Simons Foundation Principles of Microbial Ecosystems (PriME).

AUTHOR CONTRIBUTIONS

HY, GWT and VJO designed the study. HY performed geochemical analyses. MA developed the ANME-2a FISH probe. HY and GLC performed the FISH-nanoSIMS experiments and analyses. HY, CTS and AOL performed the metagenomic and metatranscriptomic experiments and analyses. HY and VJO wrote the manuscript with contributions from other authors. All authors reviewed, revised, and approved the final manuscript.

Declarations (Ethics)

COMPETING INTERESTS

The authors declare no competing interests.

ADDITIONAL INFORMATION

Supplementary information The online version contains supplementary material available at <https://doi.org/10.1038/s41396-021-01047-0>.

Correspondence and requests for materials should be addressed to V.J.O.

Reprints and permission information is available at <http://www.nature.com/reprints>

Publisher's note Springer Nature remains neutral with regard to jurisdictional claims in published maps and institutional affiliations.